Simulation for channel electrodes

Thomas Holm[a], Svein Sunde[a], Frode Seland[a], David A. Harrington[*,b]

[a]*Department of Materials Science and Engineering, Norwegian University of Science and Technology, NO-7491 Trondheim, Norway.*
[b]*Department of Chemistry, University of Victoria, Victoria, British Columbia, V8W 3V6, Canada.*

Abstract

A method for simulating electrode reactions in channel flow is developed and efficiently implemented in the symbolic algebra program Maple^{TM}. The steady-state convective diffusion equation for fully developed 2-D laminar (Poiseuille) flow past one or more electrodes in a channel is considered for a charge-transfer electrode reaction between two soluble species. The case where axial diffusion (along the channel, x direction) is neglected and the diffusivities are equal has an exact solution as an infinite series, in which each term is the product of an exponentials in x and a confluent hypergeometric function in y (across the channel). The practical implementation consists of evaluating a finite number of terms and numerically evaluating the two parameters in each term. Sturm-Liouville (eigenfunction) theory is used to reliably find the parameters for arbitrary values of the rate constants. Comparison is made with results from a commercial software package that uses a finite-element method.

Key words: channel electrodes, simulations, symbolic algebra, eigenfunctions, Sturm-Liouville, Maple

Comsol?

Introduction

The application of eigenfunction methods for the solution of convective-diffusion equations relevant to electrochemistry has a long history. The solution to the Graetz problem, which solves heat transfer to the walls of a tube with laminar flow, was given as an eigenfunction expansion as early as 1883, and an extensive treatment of the electrochemical version was given by Newman [1]. In the context of mass transport in the rectangular channels that we consider here, Moldoveanu and Anderson solved the limiting current case in terms of a series of parabolic cylinder functions [2]. In these cases, the general case of arbitrary rate constants was not attempted, perhaps because a reliable way of locating the eigenvalues was not available. Recently, Schmachtel and Kontturi used eigenfunction methods to numerically solve chronoamperometry currents at the rotating disk electrode [3]. They considered the case of arbitrary rate constants and also showed that the case of quasireversible electrode reactions could be solved as easily as the case of irreversible reactions.

*Corresponding author. Tel.: +1-250-721-7166
Email addresses: thomas.holm@ntnu.no (Thomas Holm), svein.sunde@ntnu.no (Svein Sunde), frodesel@material.ntnu.no (Frode Seland), dharr@uvic.ca (David A. Harrington)
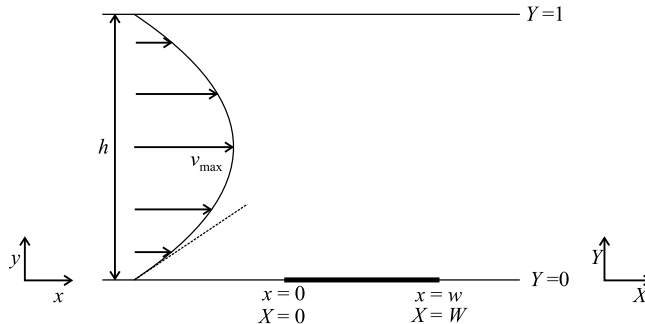
frodesel@ntnu.no

Figure 1: Notation. Flow is from left to right, with one or more embedded electrodes (bold) in the bottom of the channel. Lower case variables are dimensioned, upper case variables are nondimensionalized. The dashed line is the velocity profile (extending to infinite height) for the Lévêque approximation.

Here we apply the eigenfunction expansion method to 2-D steady-state flow past electrodes in a channel, and compare with the more conventional finite-element (FE) method, as implemented in Comsol Multiphysics®. The eigenfunction solution is a weighted sum of functions, with the functions spanning across the channel and along the electrode. That is, it is a mesh-free method and so should give good accuracy at the beginning of the electrode, where there is a step change in boundary conditions and the current density is high. Furthermore, the concentration profile, once determined, can be easily manipulated term by term to find local current densities, average current densities, or collection efficiencies, without significant degradation in accuracy. The accuracy is determined by the number of terms processed, and calculation of additional terms allows the global error to be estimated. The case where axial diffusion (along the channel) is neglected has an exact solution as an eigenfunction expansion and is investigated here.

1. Theory

We consider a solution of the steady-state diffusion-convection problem in a 2-D channel with fully developed laminar (Poiseuille) flow. Notation is given in Fig. 1. The electrode reaction (1) between two solution species has the current density at a particular location at the electrode given by the usual rate law (2). The potential at the electrode is fixed, so the rate constants (m s^{-1}) do not vary over the electrode surface. However, we allow the possibility of many electrodes along the wall of the channel, and the potential and rate constants may be different at each. The convective diffusion equation to be solved for each species is Eq. (3). We make the common assumption that the diffusivities of the two species are equal.

2

$$R \underset{k_b}{\overset{k_f}{\rightleftarrows}} P + e^- \tag{1}$$

$$j(x) = Fv(x) = Fk_f c_R(x,0) - Fk_b c_P(x,0) \tag{2}$$

$$0 = D\frac{\partial^2 c_i(x,y)}{\partial y^2} - \frac{4v_{max}}{h^2} y(h-y)\frac{\partial c_i(x,y)}{\partial x}, \;\; i = R, P \tag{3}$$

Matching of the fluxes at the electrode surface to the reaction rate leads to the boundary conditions (4) at the electrode surface. (The convective flux at the walls is zero, so only the diffusive part needs to be considered.) The flux at insulating sections between electrodes and at the top of the channel is zero, Eqs. (5) and (6). The "initial" condition is that the concentrations take the bulk values at a location x_0 upstream of the first electrode, Eq. (7). In the absence of axial diffusion, the solution only propagates downstream, and there is no loss in taking $x_0 = 0$. The measured current density is given by averaging over the electrode surface, Eq. (8).

$$D\left(\partial c_R(x,y)/\partial y\right)_{y=0} = -D\left(\partial c_P(x,y)/\partial y\right)_{y=0} = v(x) \tag{4}$$

$$\left(\partial c_R(x,y)/\partial y\right)_{y=0} = \left(\partial c_P(x,y)/\partial y\right)_{y=0} = 0 \tag{5}$$

$$\left(\partial c_R(x,y)/\partial y\right)_{y=h} = \left(\partial c_P(x,y)/\partial y\right)_{y=h} = 0 \tag{6}$$

$$c_i(x_0, y) = c_i^b, \;\; i = R, P \tag{7}$$

$$j_{ave} = (FD/w)\int_0^w \left(\partial c_R(x,y)/\partial y\right)_{y=0} \mathrm{d}x \tag{8}$$

As disscussed below, the quasireversible solution including the back reaction can be simply derived from the irreversible solution with apparent rate constant $k = k_f + k_b$, so we need only develop a numerical method for the irreversible case. We change to dimensionless variables (see Fig. 1): $Y = y/h$, $X = x/h$, $W = w/h$, $C(X,Y) = c_R(x,y)/c_R^b$, $K = hk_f/D$, $J = \left(h/c_R^b DF\right)j$ and $A = 4v_{max}h/D = 6Pe$ where $Pe = v_{ave}h/D = 2v_{max}h/3D$ is a Péclet number for mass transfer. The convective diffusion equation and boundary conditions are now

$$0 = \frac{\partial^2 C(X,Y)}{\partial Y^2} - AY(1-Y)\frac{\partial C(X,Y)}{\partial X} \tag{9}$$

$$\left(\partial C(X,Y)/\partial Y\right)_{Y=0} = KC(X,0) \text{ (at electrode)} \tag{10}$$

$$\left(\partial C(X,Y)/\partial Y\right)_{Y=0} = 0 \text{ (between electrodes)} \tag{11}$$

$$\left(\partial C(X,Y)/\partial Y\right)_{Y=1} = 0 \text{ (top of channel)} \tag{12}$$

$$C(0,Y) = 1 \text{ (upstream)} \tag{13}$$

Writing $C(X,Y) = F(X)G(Y)$ and rearranging gives Eq. (14), which shows that the partial differential equation is separable. The general solution, Eq. (15), is a superposition of products of exponential functions of X and functions

3

of Y that satisfy the differential equation (16).

$$\frac{1}{Y(1-Y)G(Y)}\frac{\mathrm{d}^2 G(Y)}{\mathrm{d}Y^2} = \frac{A}{F(X)}\frac{\mathrm{d}F(X)}{dX} = -b^2 \tag{14}$$

$$C(X,Y) = \sum_{i=1}^{\infty} a_i \exp(-b_i^2 X/A)G_i(Y) \tag{15}$$

$$G''(Y) - b^2 Y(1-Y)G(Y) = 0 \tag{16}$$

Here the prime refers to differentiation with respect to Y, and $G_i(Y)$ is an eigenfunction, i.e., a solution to Eq. (16) for $b = b_i$ where the b_i^2 are the eigenvalues. The eigenvalues are values of b^2 in Eq. (16) that satisfy boundary conditions at the electrode surface. In all cases, the solutions $G(Y)$ of Eq. (16) are chosen to satisfy the zero-flux boundary condition Eq. (17) at the top of the channel, which ensures that the concentration satisfies the zero-flux condition (12). The solutions $G(Y)$ are given in terms of confluent hypergeometric functions in Appendix A.

$$G'(1) = 0 \tag{17}$$

Three subcases are considered depending on the type of boundary condition at the $Y = 0$ surface, i.e., the electrode surface or an insulating surface between electrodes. Consider first the limiting current boundary condition, where the concentration is zero at the electrode surface, Eq. (18). Solving this for b leads to the series of values

$$G(0) = 0 \tag{18}$$

$$b_i^{(\infty)} = 3.819, 11.897, 19.924, ... \tag{19}$$

$$b_i^{(\infty)} \sim \frac{\pi(i - \frac{1}{2})}{\int_0^1 \sqrt{Y(1-Y)}dY} = 8\,(i - 1/2) \tag{20}$$

where the ∞ denotes an infinite rate constant ($K = \infty$). Formula (20) for the eigenvalues is from Sturm-Liouville theory [4], and although it is an asymptotic formula for large i, closer inspection shows that it works well also for small i. This means that these values can be used as initial estimates for the numerical solver. More precisely, the solutions are bracketed between successive values of $8i$.

Consider now the boundary condition for an insulating section of the channel or for zero current at the electrode, where the flux is zero, Eq. (21). Here the eigenvalues are given by Eq. (22).

$$G'(0) = 0 \tag{21}$$

$$b_i^{(0)} = 0, 9.052, 17.149, 25.191, ... \sim 8(i - 1) \tag{22}$$

The last case is the Robin boundary condition of Eq. (23), where K is the dimensionless rate constant. Here the eigenvalues satisfy the inequalities of Eq.

(24).

$$G'(0) - KG(0) = 0 \qquad (23)$$

$$8(i-1) < b_i^{(0)} < b_i^{(K)} < b_i^{(\infty)} < 8(i-1/2) \qquad (24)$$

For all cases, b_i lies between $8(i-1)$ and $8(i-1/2)$. (For negative K, a non-physical case, the b_i values lie between $8(i-1/2)$ and $8i$.)

The coefficients a_i are determined by the "initial" concentration profile at $X = 0$, the upstream edge of the electrode. From Eq. (15), a given initial profile $C(0, Y) = f_0(Y)$ (not necessarily $C(0, Y) = 1$) is a linear combination of the eigenfunctions $G_i(Y)$, and the coefficients can be found using the orthogonality of the eigenfunctions as

$$a_i = \frac{\int\limits_0^1 Y(1-Y) f_0(Y) G_i(Y) \, \mathrm{d}Y}{\int\limits_0^1 Y(1-Y) G_i(Y)^2 \, \mathrm{d}Y} \qquad (25)$$

Once the numerical values of the a_i and b_i have been calculated for the chosen number of terms N, the series form of the concentration, Eq. (15), is easy to manipulate. For example, the dimensionless current density averaged over an electrode running from $X = 0$ to $X = W$ is

$$J_{\mathrm{ave}} = \frac{1}{W} \int_0^W \left. \frac{\partial C}{\partial Y} \right|_{Y=0} \mathrm{d}X \qquad (26)$$

and may be calculated term by term, giving

$$J_{\mathrm{ave}} = \frac{A}{W} \sum_{i=1}^{\infty} \frac{a_i}{b_i^2} \left[1 - \exp(-b_i^2 W/A) \right] G_i'(0) \qquad (27)$$

where $G_i'(0)$ may be evaluated using the differentiation rule Eq. (40).

1.1. Multiple electrodes

The case of multiple electrodes and gaps between them is handled similarly. The solution for the first electrode proceeds as described above, with $f_0(Y) = 1$. This solution at the downstream edge of the electrode is just used as the initial profile that replaces $f_0(Y)$ in the solution of the next "segment". For example, a three-segment configuration might have segment 1 as an electrode between $X = 0$ and $X = 1$, segment 2 as an insulator between $X = 1$ and $X = 2$ with a no-flux boundary condition at $Y = 0$ and then segment 3 as an electrode after $X = 2$. The segment 1 solution $C(1, Y) = f_1(Y)$ is used as the initial profile for segment 2, and the segment 2 solution $C(2, Y) = f_2(Y)$ is used as the initial profile for segment 3.

5

2. Methods

2.1. Maple

A procedure *chsolve* to implement the above algorithm was written in the symbolic algebra system Maple$^{\text{TM}}$ [5]. The code and examples of its use are available as supplementary material, see Appendix B. The procedure takes as inputs: (i) the numerical value of the non-dimensionalized rate constant. As above, "0" indicates the zero flux condition and "infinity" indicates the case of zero concentration at the electrode surface, (ii) the name of a procedure that evaluates the initial concentration profile $f_0(Y)$, (iii) the value of A, and (iv) the number of terms N required in the eigenfunction expansion (15). The output is a procedure that evaluates the dimensionless concentration as a function of X and Y, which can then be plotted, differentiated or otherwise manipulated to produce derived quantities.

The case of multiple segments is handled by giving the rate constant as a piecewise function of X. In the single segment case, A can be left as a symbol, and then the output concentration and quantities derived for it can be plotted as a function of A. For the multisegment case, the numerical value of A must be given; this restriction arises from the need to numerically evaluate the integrals in Eq. (25) to find the concentration profile at the beginning of second and subsequent segments.

The limiting factor is the efficient numerical calculation of the integrals in Eq. (25). When the accuracy requested (via the "Digits" variable) is low, Maple works in hardware double precision arithmetic and uses the Numerical Algorithms Group routine "d01akc". For higher accuracy, Maple works in arbitrary precision arithmetic, and uses an adaptive Gaussian quadrature routine "_Gquad".

2.2. Comsol

The case of a single electrode of width $W = 1$ under limiting current conditions was also solved using Comsol Multiphysics® [6], with the conditions chosen as close as possible to those used in Maple. To effectively non-dimensionalize the problem, the problem was solved in base SI units with the parameters h, w, D and c^{b} set to unity. The problem was solved for both species using the PARDISO solver, and the A value was changed parametrically to get the solution at different flow rates. The outlet was put 10 electrode widths downstream of the electrode to eliminate the influence of the boundary condition. The outlet boundary condition is given in Eq. (**??**)

$$D_i \frac{\partial c_i}{\partial x} = 0$$

To solve for the limiting current case, the rate constant K was set to a high value (10^{10}) to effectively get a concentration of zero at the electrode. The surface concentration was verified post-calculation to be zero. Comsol does not allow the concentration at a point to have two values, as is the case for Maple at

6

the upstream edge of the electrode. To solve the problem as closely as possible to the Maple solution, the start of the geometry was set to 1/16000 of the electrode width upstream of the electrode. Here, the concentration was set to the inlet concentration, $C = 1$. This gives one mesh point (geometry determined) in distance between the concentration of 1 at the inlet to the concentration of 0 at the electrode start. The absence of axial diffusion was achieved by using anistropic diffusivities with zero X components.

The standard triangular meshing was used. A fine mesh was used at the inlet and along the electrode surface. This was set to 1/500 of the dimensionless diffusion layer thickness $\Delta = \delta/h$ estimated in the Lévêque approximation, Eq. (28).

$$\Delta = 2.83 \, (W/A)^{1/3} \tag{28}$$

for $A = A_{\max}$, where $A_{\max}$ is the highest A value that is evaluated. The mesh was allowed to grow at a rate of 5% out from the inlet and electrode surface.

3. Results

Examples of the capabilities of this method are given here, with the calculation details given in a Maple worksheet in the supplementary material, see Appendix B.

3.1. Irreversible Reaction

The case of $K = K_{\mathrm{f}} = 10$ for $A = 100$ (Péclet number 16.7) is illustrated in Fig. 2. The consumption of the species at the electrode is seen, and its variation along the electrode surface. The increasing thickness of the diffusion layer is also evident, and by $X = 2$, the concentration at the top of the channel is significantly diminished from its initial value of 1. Small ripples in the Y direction close to $X = 0$ are the Gibbs' phenomenon, well known in Fourier theory, which is a special case of the Sturm-Liouville theory applicable here.

3.2. Flow rate dependence of limiting current

The limiting current density is found from the flux via Eq. (27), for the case of the boundary condition $C(X, 0) = 0$ or Eq. (18). The series (27) has numerical values of the a_i and b_i but A and W are still arbitrary, and so the limiting current as a function of flow rate may be readily plotted and compared with the Comsol results as in Fig. 3. For comparison, two approximate relationships are also shown: (i), the limiting current given by the Levich equation, Eq. (29), and (ii), the complete consumption or "thin layer" limit, Eq. (30).

$$J_{\mathrm{ave}}(\mathrm{Levich}) = \left(3^{4/3}/2\Gamma\,(1/3)\right) (A/W)^{1/3} \tag{29}$$

$$J_{\mathrm{ave}}(\mathrm{thin\ layer}) = A/6 \tag{30}$$

The Levich equation for limiting current assumes not only the absence of axial diffusion, but also the Lévêque approximation for the velocity profile (see Fig.

7

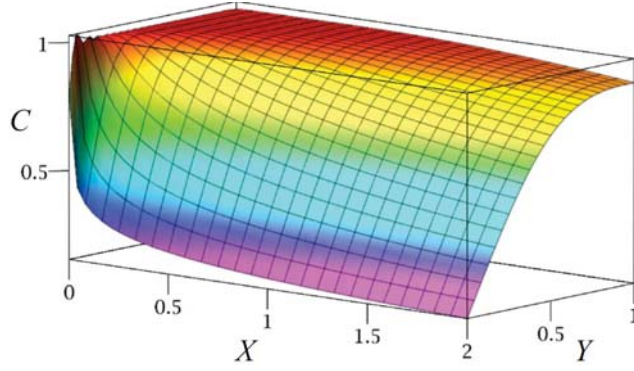Figure 2: Concentration profile for an irreversible reaction. $K_\mathrm{f} = 10$, $A = 100$. Series evaluated to 40 terms.
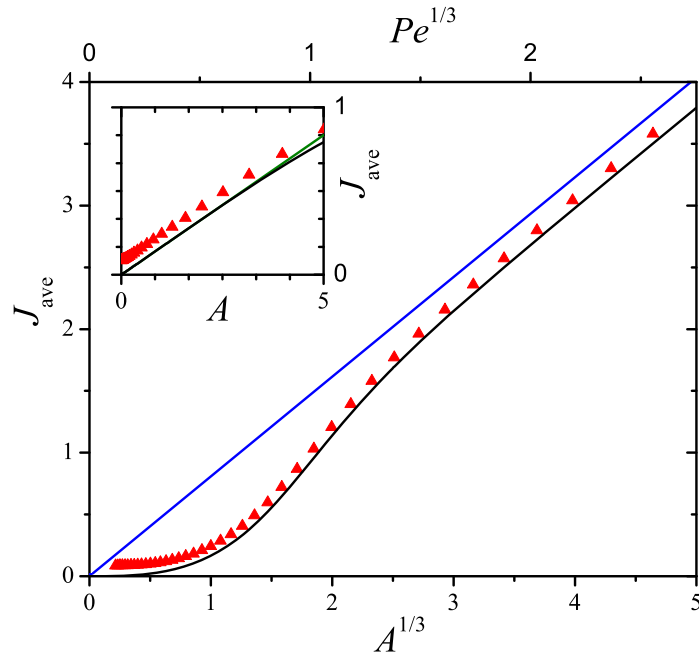

Figure 3: Current density dependence on flow rate. Limiting current $(C = 0)$ boundary condition, for $W = 1$. $A = 6Pe$ is a dimensionless flow rate. Comparison of Maple 40 term eigenfunction solution (black line) and Comsol solution (red triangles). Main figure compares these with the $A^{1/3}$ dependence of the Levich approximation (blue line, Eq. (29)); inset compares with complete consumption approximation (green line, Eq. (30)).

1). The latter approximation is valid only when diffusion is confined to close to the electrode and this approximation should be approached at high flow rates. The current density tends to zero as A tends to zero at fixed W as predicted by Eq. (27). At the lowest flow rates, the reactant is completely consumed before it reaches the downstream edge of the electrode. In this case the total moles reacting per second at the electrode must equal the total moles per second entering the channel, which leads to the thin layer limit of Eq. (30). The behavior and comparison of the curves is further discussed below.

3.3. Quasireversible reactions

For the case where the redox reaction (1) is quasireversible with rate law (2), we nondimensionalize similarly to before, assuming the diffusivities are equal and that the product concentration is initially zero.

$$S = c_P / c_R^b \tag{31}$$

$$
\begin{aligned}
-(\partial S(X,Y)/\partial Y)_{Y=0} &= (\partial C(X,Y)/\partial Y)_{Y=0} \\
&= (hk_f/D)\,C(X,0) - (hk_b/D)\,S(X,0) \\
&= K_f C(X,0) - K_b S(X,0)
\end{aligned}
\tag{32}
$$

For the case of equal diffusivities, the principle of unchanging total concentration applies [7], which means that $c_R + c_P = c_R^b$ everywhere in the channel, or equivalently $S(X,Y) = 1 - C(X,Y)$. Under this condition, it is possible to easily derive the quasireversible solution from the irreversible one [8]. This means that only one mass-transport problem needs to be solved. The quasireversible concentrations are given by Eqs. (33) and (34), where $C_{ir}^{(K_f+K_b)}$ means the solution to the irreversible problem with rate constant $K_f + K_b$.

$$C(X,Y) = (K_f C_{ir}^{(K_f+K_b)}(X,Y) + K_b)/(K_f + K_b) \tag{33}$$
$$S(X,Y) = 1 - C(X,Y) \tag{34}$$

That is, the eigenfunction solution is found for boundary condition (23) with $K = K_f + K_b$, and then substituted into these equations. Eq. (26) then gives the quasireversible current density. Examples of steady-state current potential curves calculated in this way are given in Fig. 4. The fast reaction case of $K^\circ = 100$ can be checked against the behaviour expected for a reversible reaction, and the current density is indeed half the limiting value at $E_{1/2} = E^\circ$.

If the product is initially present with concentration c_P^b, then c_R^b is replaced by $c_P^b + c_R^b$ in the definitions of C and S and the revised rule is given by Eq. (35), where $f = c_R^b/(c_P^b + c_R^b)$. An example is given in the supplementary material.

$$C(X,Y) = \frac{C_{ir}^{(K_f+K_b)}(X,Y)\,(fK_f - (1-f)K_b) + K_b}{K_f + K_b} \tag{35}$$

9
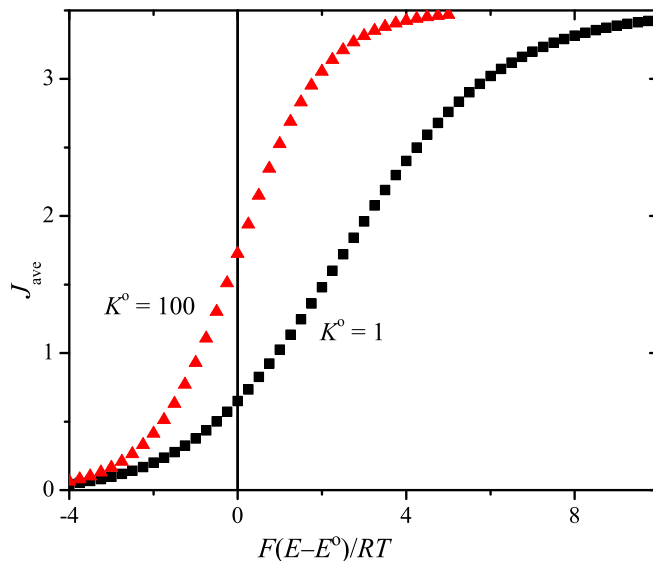
Figure 4: Steady-state current potential curves. Quasireversible reaction, $\beta = 0.5$ $W = 1$, $A = 100$, 40 terms.

3.4. Collection efficiency

The collection efficiency may be calculated as the ratio of the current at an upstream electrode where the reaction occurs under limiting current conditions, to the current at a downstream electrode where the reverse reaction occurs under limiting current conditions. First a two-segment calculation is carried out for the concentration C with boundary condition $K = \infty$ ($C = 0$) for the first segment (upstream electrode) and $K = 0$ (zero-flux) for the second segment (gap between the two electrodes). The concentration S at the end of the second segment is calculated as $1 - C$ under the assumption that the diffusivities are equal, and this is then used as the initial concentration profile for the calculation of the concentration S for the third segment (second electrode) with boundary condition $K = \infty$ ($S = 0$). Integration of the local current densities over the two electrodes gives the two currents, whose ratio is the collection efficiency. Fig. 5 shows an example where the electrode widths and the gap are all equal and $A = 100$. This collection efficiency here, 0.295, is higher than the value using the standard calculation, 0.250, which assumes the Lévêque approximation [9]. This is because at this flow rate, a significant amount of the product has diffused across the channel, and its reflection back enhances the collection efficiency.
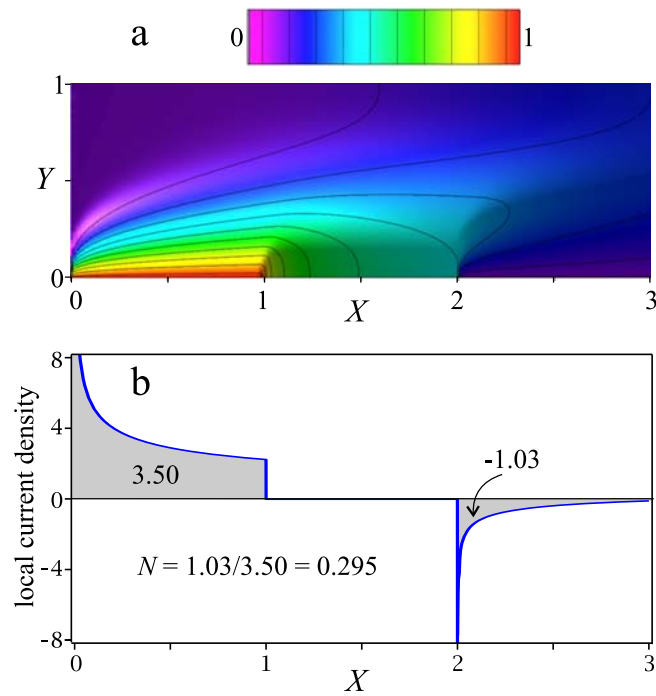
10

Figure 5: Collection efficiency calculation. (a) Concentration of product. Limiting current production at electrode between $X = 0$ and $X = 1$ and limiting current consumption at electrode between $X = 2$ and $X = 3$ (40 term calculation). Contours are at 0.05, 0.15, ..., 0.95. (b) Local dimensionless current density along the channel, and calculation of efficiency from the shaded areas.

4. Discussion

4.1. Accuracy and convergence

The limiting current case is the most difficult of the cases from a numerical point of view, and so we begin with a discussion of the results in Fig. 3. The Comsol results, intended as a verification strategy, do not agree with the Maple results using 40 terms. Increasing to 100 terms makes only a 0.3% difference at the highest flow rate shown on the plot. There appears to be a constant systematic error in the Comsol results. This is confirmed by looking at the low flow rate regime, where the Maple behaviour correctly gives $J_{ave} = A/6$, but Comsol has a constant offset, and does not go to zero at zero flow rate, which is the correct limit in the absence of axial diffusion. This is attributed to the use of triangle meshes that do not align with the X and Y directions, and lead to a small amount of "numerical diffusion" in the X direction even when axial diffusion was nominally precluded. Use of a rectangular mesh aligned with the X and Y directions was attempted to solve this problem, but expanding meshes do not maintain alignment and fixed fine meshes run into memory limitations, and so this was strategy was not pursued further.

Convergence issues of the eigenfunction method did become significant at higher flow rates than shown in Fig. 3, where the separation from the Levich line increased. Increasing the number of terms improved the situation, in that the point of divergence was delayed to higher flow rates, but ultimately it is simply more accurate to use the Levich fomula.

For the more general case of finite rate constants, the accuracy of the method was investigated over a wide parameter space. A criterion for adequate convergence was taken as less than 0.1% change on increasing the number of terms by 10. It is difficult to prove that this represents absolute convergence, but it enables the trends to be found, and gives reasonable confidence that the results are correct at the 1% level. Parameters investigated were: (i) K from 10^1 to 10^7 by factors of 10, and ∞, (ii) numbers of terms from 10 to 100 in steps of 10, (iii) A values from 1 to 10^5 in a 1-3-10 sequence. This study led to the following conclusions:

1. Convergence is easier to reach (at a lower number of terms) for lower K values.

2. Convergence is faster at lower A values and/or lower K.

3. For $K \geq 10^5$, the results for 10 or more terms are all within 0.1 % of the $K = \infty$ value.

4. For a given K value, the change from 90 to 100 terms leads to less than 0.1 % change for all A values except for the two largest. The two largest A values only reach this criteria for the two smallest K values.

5. The calculation time is mainly dependent on the number of terms used (and less on the K or A value), but this effect is small enough that 100 terms can be practically calculated as a matter of routine. The calculation time for 100 terms was comparable to the Comsol calculation time.

12

Although Maple allows for arbitrary precision calculations, the hardware double precision calculations were found to be sufficient for 100 term calculations, i.e., the accuracy is limited by the number of terms and not the accuracy of the calculation engine.

For multisegment calculations, the calculation time for second and subsequent segments was significantly higher than for the first segment, because of the large number of hypergeometric function evaluations needed in the integrals in the a_i coefficients, Eq. (25). This can be remedied by numerically fitting the concentration profile at the end of a segment to a suitable function, and using that as the initial concentration profile for the next segment. Strictly, this means that the guarantee of higher accuracy with more terms (provided by Sturm-Liouville theory) is invalidated. However, least-squares fitting of the concentration profile at 101 points across the channel to a degree 10 polynomial decreased the calculation time for the second segment to approximately the same time as the first segment without a noticeable change in accuracy (see the collection efficiency calculation in the supplementary material).

4.2. Method assessment

Most analytical solutions for concentrations or currents in channel electrodes have used the Lévêque approximation, and neglected axial diffusion, e.g., these are standard approximations in calculating collection efficiencies [9–11]. These approximations work best at fast flow rate and large channel heights. There has been some consideration of the effects of axial diffusion [1, 12–14], and more recently Amatore and coworkers [15] have mapped out the zone diagram for the various limiting and intermediate cases in terms of the parameters W and Pe. The present work neglects axial diffusion but goes beyond the Lévêque approximation and considers the full velocity profile across the channel. This approximation works well for intermediate flow rates and small channel heights. [**Need more comparison with literature here, or more specifiy criterion?**]. The collection efficiency calculation above indicates that the error in using the Lévêque approximation for small channel heights can be significant.

The present work indicates that extending the solution all the way across the channel is not significantly more difficult than the Lévêque approximation. Like the semidifferentiation approach of Oldham for planar electrodes [16] or the Laplace transform method that implements the far boundary condition, the present method exactly solves the problem across the channel and the reduces the problem to solving along the near surface of the channel. It is to be emphasized that the eigenfunction expansion is an exact solution to the problem without axial diffusion, and the only approximation arises from the need to solve for the eigenvalues and coefficients numerically, and to terminate the series after a finite number of terms. There are standard methods for using eigenfunction expansions that may be used in problems that include axial diffusion, i.e., for elliptic partial differential equations [17], which will be explored in subsequent work. That is, the present confluent hypergeometric functions may be a suitable basis set for the more general case, but the complexity of the method will be significantly greater, and an iterative method may be required.

13

In terms of a numerical method, the eigenfunction expansion method used here has the advantage over FE or finite-difference methods that mesh optimization, with a strategy for finer meshes near electrodes and electrode edges, is not required. On the other hand, eigenfunction expansion methods are known for slow convergence. Perhaps not surprisingly, we find that the conditions that require a fine, adaptive mesh for FE solution such as large flow rates, are also the conditions that require more terms for acceptable convergence in our method. Accurate convergence was possible for comparable computational expense as for the FE method, but the present method is algorithmically much simpler and the global error is more easily assessed. An important advantage of the present method is that a whole segment is solved at one time, so the complexity of the calculation is largely independent of the channel height or width of the electrode.

In principal the present method did not require a symbolic algebra system for its implementation. Such systems allow arbitrary precision calculations, but this feature was not found to be necessary here. These systems do have an important advantage in processing the concentration profile into the required measurable quantities, such as average current density or collection efficiency. This processing typically involves differentiation or integration, which is done exactly by simple rules such as the differentiation rule (40), and does not degrade the accuracy of the calculation.

Another advantage of these systems is that the numerical evaluation of the hypergeometric and exponential functions in the solution is deferred until they are needed. In Fig. 2, for example, Maple's plot routine decides where to evaluate the concentrations, using more points in steeper regions of the plot. The numerical evaluation of these concentrations occurs in the plot routine itself, and not in the construction of the series solution. Therefore, there is no need for evaluate the solution over a fine grid of points just in case they might be required later. This is perhaps seen most clearly in the case of a single electrode, where the limiting current can be given as a function of an unspecified A, and then this function is used to create Fig. 3.

Coupled with the advances in computing speed, these advantages of symbolic algebra programs mean that reconsideration of algorithms such as the eigenfunction method demonstrated here may lead to competitive numerical methods with high accuracy that are simple to implement.

A. Solution of ODE for $G(Y)$

The differential equation (16) has the general solution Eq. (36) with two arbitrary constants g_1 and g_2.

$$G(Y) = g_1 G_1(Y) + g_2 G_2(Y) \tag{36}$$
$$G_1(Y) = \exp\left(bY(1-Y)/2\right)$$
$$\times {}_1F_1\left(1/4 - b/16; 1/2; b(2Y-1)^2/4\right) \tag{37}$$
$$G_2(Y) = \exp\left(bY(1-Y)/2\right)(2Y-1)$$
$$\times {}_1F_1\left(3/4 - b/16; 3/2; b(2Y-1)^2/4\right) \tag{38}$$

Other notations for the confluent hypergeometric functions ${}_1F_1\left(a; b; z\right)$ are ${}_1F_1\left({a \atop b}; z\right)$ or $M(a, b, z)$ [18]. It is evident that $G_1(Y)$ is symmetric (even) about $Y = 1/2$ and $G_2(Y)$ is antisymmetric (odd) about this point. Applying the no-flux boundary condition at the top of the channel, $G'(1) = 0$, allows determination of one of the constants, and the other is chosen to scale the functions so that $G(1) = 1$, with the result Eq. (39).

$$G(Y) = \frac{G_2'(1)G_1(Y) - G_1'(1)G_2(Y)}{G_2'(1)G_1(1) - G_1'(1)G_2(1)} \tag{39}$$

The derivatives with respect to Y are readily evaluated using the differentiation rule

$${}_1F_1\left(c; d; f(Y)\right)' = \frac{c}{d}\,{}_1F_1\left(c+1; d+1; f(Y)\right)f'(Y) \tag{40}$$

According to Sturm-Liouville theory, the eigenfunctions $G_i(Y)$ for different values of b_i that satisfy the boundary conditions are orthogonal with respect to the weight function $Y(1-Y)$:

$$\int_0^1 Y(1-Y)G_i(Y)G_j(Y)\,\mathrm{d}Y = 0, \ i \neq j \tag{41}$$

B. Supplementary material

Supplementary material consists of a Maple worksheet that implements the algorithm here and applies it in several examples, a .pdf file of this worksheet, and a text file with the Maple code for the chsolve procedure. This material can be found, in the online version, at http://dx.doi.org/10.1016/j.jelechem.XXXX.

References

[1] J. Newman, in Electroanalytical Chemistry, Ed: A. Bard, Marcel Dekker, NY, 1973, v. 6, p. 187, Sec. XVII.

[2] S. Moldoveanu, J.L. Anderson, J. Electroanal. Chem. 175 (1984) 67, doi:10.1016/S0022-0728(84)80346-0.

[3] S. Schmachtel, K. Kontturi, Electrochim. Acta. 56 (2011) 6812, doi:10.1016/j.electacta.2011.05.087.

[4] J.L. Troutman, M. Bautista, Boundary Value Problems of Applied Mathematics, PWS Publishing, Boston, 1994.

[5] Maple v 18.01, Maplesoft, a division of Waterloo Maple Inc., Waterloo, Ontario, http://www.maplesoft.com.

[6] COMSOL v. 4.4, Comsol Inc, Burlington, MA, http://www.comsol.com.

[7] K.B. Oldham, S.W. Feldberg, J. Phys. Chem. B 103 (1999), 1699, doi:10.1021/jp9837939.

[8] D.A. Harrington, Electrochim. Acta, in press, doi:10.1016/j.electacta.2014.11.101.

[9] C.M.A Brett and A.M.C.F. Oliveira-Brett, Hydrodynamic Electrodes, in Comprehensive Chemical Kinetics, Eds. C.H. Bamford and R.G. Compton, Elsevier, Amsterdam, 1986, v 26, p. 355.

[10] R. Braun, J. Electroanal. Chem., 19 (1968) 23.

[11] J.A. Cooper, R.G. Compton, Electroanalysis, 10 (1997) 141.

[12] K. Aoki, K. Tokuda, H. Matsuda, J. Electroanal. Chem. 217 (1987) 33.

[13] R.G. Compton, A.C. Fischer, R.G. Wellington, P.J. Dobson, P.A. Leigh, J. Phys. Chem. 97 (1993) 10410.

[14] J.A. Alden, R.G. Compton, J. Electroanal. Chem., 404 (1996) 27.

[15] C. Amatore, N. Da Mota, C. Sella, L. Thouin, Anal. Chem. 79 (2007) 8502.

[16] J.B. Oldham, J.C. Myland, A.M. Bond, Electrochemical Science and Technology: Fundamentals and Applications, Wiley, Chichester, U.K., 2012.

[17] D. Zwillinger, Handbook of Differential Equations, 2nd Ed. Academic Press, San Diego, 1992, Sec. II.A.54.

[18] F.V. Olver, D.W. Lozier, R.F. Boisvert, C.W. Clark, (Eds.), NIST Handbook of Mathematical Functions, NIST and Cambridge University Press, NY, 2010, Sec. 13.14. Online version at http://dlmf.nist.gov/.